Buoyancy Flux Modeling for Cloudy Boundary Layers

D. C. LEWELLEN AND W. S. LEWELLEN

West Virginia University, Morgantown, West Virginia

(Manuscript received 17 June 2003, in final form 3 December 2003)

ABSTRACT

The modeling of the buoyancy flux in a partly cloudy atmospheric boundary layer is complicated by its dependence on the correlation between clouds and vertical velocity elements, which can vary significantly with the underlying layer dynamics (e.g., stratocumulus versus shallow cumulus). The buoyancy flux is sometimes modeled in terms of higher-order statistics, such as vertical velocity skewness or saturation variance, to try to capture some of these dynamical effects. In this work an approximate expression for the buoyancy flux is formulated solely in terms of the liquid potential temperature and total water profiles and their respective flux profiles. The predictions compare favorably with the results of an extensive set of large-eddy simulations (LES), including simulations of stratocumulus, shallow cumulus, and transitional behavior in between. This formulation is combined with previous results on the relation between cloud-top entrainment rate and circulation structure to predict the behavior of quasi-steady cumulus-coupled boundary layers as a function of a basic set of physical input parameters. These predictions also compare favorably with LES results.

1. Introduction

Individual cloud elements cannot generally be resolved by grids used in mesoscale (or larger) meteorological models, so subgrid parameterization of partly cloudy atmospheric boundary layers has been a longstanding subject for research. Regardless of the sophistication used in modeling the dynamics of partly cloudy layers, some representation of the horizontal mean buoyancy flux in terms of the fluxes of adiabatically conserved variables, for example, total water mixing ratio, q_t, and liquid potential temperature, θ_l, is usually required.

To a good approximation the buoyancy flux[1] may be written as

$$\overline{w'\theta_v'} = (1 + 0.61q_t)\overline{w'\theta_l'} + \alpha\overline{w'q_t'} + \beta\overline{w'q_l'}, \quad (1)$$

where q_l is the liquid water mixing ratio, α and β are thermodynamic coefficients defined in appendix A, and the overbars indicate a horizontal average. Expressing the mean liquid water flux, $\overline{w'q_l'}$, in terms of the fluxes of θ_l and q_t is the chief difficulty, since this depends on how the clouds and vertical velocity are correlated locally. In the limit where a given vertical level is all clear or all cloudy this difficulty is avoided. We can define "dry" and "wet" buoyancy fluxes that, to a good approximation, equal the buoyancy flux in the limit of all-clear or all-cloudy conditions, respectively:

$$D \equiv (1 + 0.61q_t)\overline{w'\theta_l'} + \alpha\overline{w'q_t'} = \overline{w'\theta_v'} \quad \text{if all clear} \quad (2)$$

$$W \equiv (1 + 0.61q_t)\overline{w'\theta_l'} + \alpha\overline{w'q_t'} + \beta\overline{w's'} = \overline{w'\theta_v'} \quad \text{if all cloudy} \quad (3)$$

$$\approx (1 + 0.61q_t - \beta b)\overline{w'\theta_l'} + (\alpha + \beta a)\overline{w'q_t'}. \quad (4)$$

Here s is the difference between the total-water and saturation mixing ratios, which may be approximated by linearizing the saturation formula,

$$s \equiv q_t - q_s \approx aq_t' - b\theta_l' + c, \quad (5)$$

leading to the approximation in (4). Here q_s is the saturation mixing ratio and a, b, and c are thermodynamic coefficients given in appendix A.

In the general partly cloudy case we may formally write the buoyancy flux as an interpolation between the dry and wet limits,

$$\overline{w'\theta_v'} = (1 - \hat{R})D + \hat{R}W, \quad (6)$$

where, from (1) to (3), the interpolation variable $\hat{R}$ is given by,

$$\hat{R} = \frac{\overline{w'\theta_v'} - D}{W - D} = \frac{\overline{w'q_l'}}{\overline{w's'}}. \quad (7)$$

Modeling of $\overline{w'\theta_v'}$ in terms of $\overline{w'q_t'}$ and $\overline{w'\theta_l'}$ amounts to finding a representation for $\hat{R}$. One approach has been

[1] Throughout the text we refer to the virtual potential temperature flux, $\overline{w'\theta'}_v$, simply as the "buoyancy flux" for brevity.

Corresponding author address: D. C. Lewellen, MAE Dept., WVU, P.O. Box 6106, Morgantown, WV 26506-6106.
E-mail: dclewellen@mail.wvu.edu

statistical formulations relating the variances and covariances of the relevant fluctuations. Sommeria and Deardorff (1977) and Mellor (1977) assumed joint-Gaussian distributions for the probability density functions (pdfs) of the fluctuations of w, q_t, and θ_l. In this limit (in which the vertical velocity and cloud water fluctuations are uncorrelated) $\hat{R}$ is found to be identically equal to the mean partial cloud fraction, which in turn is determined as a function of the appropriate variances and covariances.

In partly cloudy conditions where latent heat release is very important to the dynamics, the vertical velocity and cloud water fluctuations tend to be strongly correlated and the actual $\hat{R}$ can depart significantly from the mean cloud fraction. The pdfs in this case are not well represented by joint-Gaussians. Bougeault (1981) found that many simulated clouds produced from large-eddy simulations (LESs) showed positively skewed conserved variable distributions better fit with exponential or gamma distributions. Under highly skewed conditions with small cloud fractions and relatively strong updrafts such as may occur in shallow cumulus, Randall (1987) demonstrated that the phenomenological updraft–downdraft model developed for tropospheric cumulus parameterization provided a much better representation than the Gaussian pdf partial cloudiness models. Lewellen and Yoh (1993) introduced a binormal formulation that provided for a smooth transition between the Gaussian distribution and a double Gaussian. In the limit of high skewness, the double Gaussian approaches the two-delta functions of the simple updraft–downdraft model. This formulation represented distributions obtained from LES results well when analyzed values of the skewness were used, but did not provide a model for the skewness.

Bechtold and colleagues have tried to empirically determine relations between the fractional cloudiness, the cloud water content, and the liquid water flux as a function of $\overline{s}/\sigma_s$, the mean saturation deficit normalized by its standard deviation. Bechtold et al. (1992) indicated that such relations based on the Gaussian distribution could produce reasonable boundary layer structure for layers with cloud fractions greater than approximately 20%. Bechtold et al. (1995) added a function to account for non-Gaussian behavior at small cloud fractions and improved upon this empirical function in Cuijpers and Bechtold (1995) and Bechtold and Siebesma (1998). In this approach $\hat{R}$ [which is equal to the combination $f_N N$ in Bechtold and Siebesma (1998)] is empirically determined as a function of $\overline{s}/\sigma_s$ from LES results.

Though the main focus in these works (and here) is partly cloudy layers (particularly shallow cumulus, stratocumulus over cumulus, and broken stratocumulus), it should be noted that even for solid stratocumulus determining $\hat{R}$ is an issue at cloud top. This is particularly important for treatments of cloud-top entrainment that require parameterizing the buoyancy flux at the inversion, $\overline{w'\theta'_{vi}}$. See, for example, Lilly (2002) for a recent treatment [$\hat{R}(z_i)$ here is his parameter α, which he estimates from LES results under the assumption that a particular parameterization for $\overline{w'\theta'_{vi}}$ holds].

Most of the preceding approaches aim to express $\hat{R}(z)$ as a function of thermodynamic moments defined locally at z. The underlying dynamics, however, is typically dominated by coherent circulations extending over much of the boundary layer depth, which, upon horizontal averaging, would naturally lead to a nonlocal result in z. Invoking higher-order moments (skewnesses, saturation variance, etc.) is done in part to try to circumvent this difficulty and provide a formulation local in z. An alternative is to actually provide a simple model for the underlying eddy dynamics. This is the case for mass flux models, where $\overline{w'\theta'_v}$ is computed directly, but this requires a specification of the convective mass flux and assumptions about lateral entrainment and detrainment in and out of the updrafts.

In the following section we formulate expressions for $\hat{R}$ incorporating nonlocality in z at a very simple level, inspired by the mass flux approach. This enables $\overline{w'\theta'_v}$ to be expressed approximately using only the most basic of inputs, the $\overline{q_t}$, $\overline{\theta_l}$, $\overline{w'q'_t}$, and $\overline{w'\theta'_l}$ profiles. This formulation was tested against LES predictions for a variety of boundary layers; the results are sampled and summarized in section 3. The LES cases include the large set of idealized layers driven by surface heat and humidity fluxes that was employed in Lewellen and Lewellen (2002, hereafter referred to as LL02), and a sample from recent LES intercomparisons organized by the Global Water and Energy Experiment (GEWEX) Cloud Systems Studies (GCSS) boundary layer clouds working group (WG1).

In section 4, $\hat{R}$ is used to extend the results of LL02 on the relation between boundary layer entrainment and circulation structure for shallow cumulus conditions. For quasi-steady conditions this allows reasonably successful predictions of cumulus-coupled layer dynamics (e.g., the fluxes, q_t and θ_l within the cloud layer) to be made as a function of a basic set of input parameters.

2. Approximating $\hat{R}$

A basic requirement of $\hat{R}$ in (6) is that it interpolate between 0 and 1 for all-clear and all-cloudy conditions, respectively. For conditions with a relatively uniform cloud base (e.g., typical stratocumulus) the details of that interpolation are not so important. The more challenging case is shallow cumulus, where $\hat{R}$ can be large even while the cloud fraction is small because the cloud elements and strong updrafts are highly correlated. Accordingly, we concentrate on developing an appropriate formulation of $\hat{R}$ for shallow cumulus and will check its adequacy for other conditions a posteriori.

As in Bechtold and Siebesma (1998) we employ the mass flux model to approximate $\hat{R}$, but do so in a dif-

ferent fashion. In general, for the flux of any scalar quantity Ψ, we have

$$\overline{w'\Psi'} \approx \nu M_c(\Psi^u - \Psi^d), \tag{8}$$

where M_c is the convective mass flux, ν is a proportionality constant, and the superscripts denote updraft and downdraft values. We apply this to (7) at what is a priori a very crude level: using the horizontal mean profiles $\overline{q_t}$ and $\overline{\theta_l}$ to define downdraft properties, and constant values q_t^{sc} and θ_l^{sc} characteristic of the lower portion of the subcloud layer to define updraft properties, giving

$$\hat{R} \approx \frac{q_l^{sc} - q_l^b}{s^{sc} - s^b}. \tag{9}$$

Here, $s^{sc}(z) = q_t^{sc} - q_s(\theta_l^{sc}, q_t^{sc}, z)$ is the saturation deficit of a parcel with values θ_l^{sc} and q_t^{sc} at height z; $q_l^{sc}(z) = q_l(\theta_l^{sc}, q_t^{sc}, z) = \max[0, s^{sc}(z)]$ is the liquid water mixing ratio of such a parcel. The variables $s^b(z) = \overline{q}_t(z) - q_s[\overline{\theta_l}(z), \overline{q}_t(z), z]$ and $q_l^b(z) = q_l[\overline{\theta_l}(z), \overline{q}_t(z), z] = \max[0, s^b(z)]$ are the corresponding quantities for a parcel at height z possessing the values $\overline{\theta_l}(z)$ and $\overline{q}_t(z)$. Note that q_l^b and s^b are not equal to the horizontal means $\overline{q_l}$ and $\overline{s}$.

Alternatively we can apply (8) to (7) in the analogous way but using the approximation (4) for W arising from the linear approximation to the saturation formula, giving

$$\hat{R} \approx \frac{\overline{w'\theta_v'} - (1 + 0.61q_t)\overline{w'\theta_l'} - \alpha\overline{w'q_t'}}{\beta(a\overline{w'q_t'} - b\overline{w'\theta_l'})} \tag{10}$$

$$\approx \frac{(\theta_v^{sc} - \theta_v^b) - (1 + 0.61q_t)(\theta_l^{sc} - \overline{\theta_l}) - \alpha(q_t^{sc} - \overline{q}_t)}{\beta[a(q_t^{sc} - \overline{q}_t) - b(\theta_l^{sc} - \overline{\theta_l})]}, \tag{11}$$

where a, b, α, β, and θ_v^b are all computed using $\overline{q}_t$ and $\overline{\theta_l}$.

The expression (9) does not involve a linearization of the saturation formula and is conceptually simpler than (11) (all the terms of which generally contribute significantly, precluding further simplification). On the other hand, by using (4) for W the buoyancy flux is given by (6) in terms of $\overline{w'\theta_l'}$ and $\overline{w'q_t'}$ alone without reference to $\overline{w's'}$, which is often convenient in practice. We use the forms (4), (10), and (11) later in comparing with our LES results, for example, because $\overline{w's'}$ was not included in the statistics stored for each run. In practice the predictions from (9) and (11) agree with each other to a within a few percent or better, with the largest differences occurring where liquid water levels are highest, at the tops of thick cloud layers.

Some further comments on these approximations to $\hat{R}$ are in order. First, since $q_l = \max(0, s)$, it is clear that (9) is 0 below cloud base and 1 in a solid cloud, as expected; indeed (9) remains bounded between 0 and 1 regardless of what $\overline{q}_t$ and $\overline{\theta_l}$ profiles (physical or unphysical) are used to evaluate it. Second, while the mass flux approximation (8) is sometimes rough and we have taken liberties with it, several sources of uncertainty drop out, at least partially, in the final expression, suggesting that the result might prove more successful than the derivation would indicate at first glance. In replacing q_t^u and θ_l^u with q_t^{sc} and θ_l^{sc} we have nominally ignored mixing between the updraft and its environment, which is not a good approximation for traditional mass flux applications to cumulus. In using (8) to get from (7) to (9) [or from (10) to (11)], however, the leading effect of this mixing—forcing updraft values toward the background ones—is common to the numerator and denominator and so at least partly cancels in the ratio. In this substitution the factors of ν and M_c that are introduced cancel exactly. Third, the resulting approximations to $\hat{R}$ are nonlocal in z but in a simple way: through the dependence, at all levels, on the near-surface subcloud values q_t^{sc} and θ_l^{sc}. Finally, the result depends only on $\overline{q}_t$ and $\overline{\theta_l}$, unlike other expressions given in the literature that depend on the horizontal mean liquid water and cloud fraction [as in the mass-flux-derived expression in Bechtold and Siebesma (1998)], the saturation deficit variance (Cuijpers and Bechtold 1995), or w-skewness and s-skewness (Lewellen and Yoh 1993).

Our search for a form with very basic ingredients was motivated in part by an empirical finding from our LES results: the instantaneous horizontal mean fluxes measured in simulations with modest domain sizes exhibited a very large degree of variability in time, but in the $\hat{R}$ measured from (10) most of this variability dropped out, suggesting the possibility of a formulation independent of higher moment quantities. To give a concrete, representative example: in simulation NHb from LL02 (cf. Figs. 2a and 6 later) the standard deviation in time of the horizontal average normalized by the time average for the heat, moisture, and buoyancy fluxes were $\sigma_{\langle w'\theta_l'\rangle}/|\overline{w'\theta_l'}| = 0.19$, $\sigma_{\langle w'q_t'\rangle}/\overline{w'q_t'} = 0.20$, and $\sigma_{\langle w'\theta_v'\rangle}/\overline{w'\theta_v'} = 0.26$, respectively, at 600-m height, while the fluctuations of $\hat{R}$ at that height were nearly an order of magnitude smaller, $\sigma_{\langle\hat{R}\rangle}/\overline{\hat{R}} = 0.027$.

One limitation of (9) or (11) is straightforwardly improved upon. The transitions at cumulus or stratocumulus cloud base occur at fixed heights instead of distributed in z because no contribution from fluctuations away from the mean updraft or mean downdraft values has been included. Assuming a Gaussian distribution of fluctuations in properties of the subcloud parcels contributing to cumulus plumes (with means q_t^{sc}, θ_l^{sc}, and standard deviations $\sigma_{q_t}^{sc}$, $\sigma_{\theta_l}^{sc}$) and in fluctuations in downdraft/background properties (means $\overline{q}_t$, $\overline{\theta_l}$, and standard deviations $\sigma_{q_t}^b$, $\sigma_{\theta_l}^b$), we can incorporate these effects to linear order in the fluctuations as described in Sommeria and Deardorff (1977) and Mellor (1977) (SDM hereafter). Note that we are considering the fluctuations about the updraft and downdraft means separately, not the contribution of the updraft–downdraft differences to the total variances (which would be poorly represented

by a Gaussian for cumulus conditions). Averaging over the appropriate ensembles in the numerator and denominator of (9) leaves the denominator unchanged and replaces q_l^{sc} and q_l^b in the numerator with the appropriate SDM expressions,

$$\hat{R} \approx \frac{q_{l,\mathrm{SDM}}^{sc} - q_{l,\mathrm{SDM}}^{b}}{s^{sc} - s^{b}}, \tag{12}$$

with

$$q_{l,\mathrm{SDM}}^{sc} = \sigma_s^{sc}\left(R^{sc}Q_1^{sc} + \frac{1}{\sqrt{2\pi}}e^{(-Q_1^{sc2})/2}\right) \tag{13}$$

$$R^{sc} = \left[1 + \mathrm{erf}\left(\frac{Q_1^{sc}}{\sqrt{2}}\right)\right]\Big/ 2 \tag{14}$$

$$Q_1^{sc} = a(q_t^{sc} - q_{sl}^{sc})/\sigma_s^{sc}, \tag{15}$$

and similarly for $q_{l,\mathrm{SDM}}^{b}$. The corresponding change is effected in (11) by adding

$$\beta(q_{l,\mathrm{SDM}}^{sc} - q_l^{sc} - q_{l,\mathrm{SDM}}^{b} + q_l^{b}) \tag{16}$$

to the numerator.

We will see in comparing with LES results later that the effects of these fluctuations on $\hat{R}$ are secondary, so rough estimates for the standard deviations of the saturation deficits, σ_s^{sc} and σ_s^b, suffice for these purposes. Here we use characteristic θ_l and q_t differences based on the surface fluxes to estimate these variances,

$$\sigma_s^{sc} = [(a\delta q_t^{sc})^2 + (b\delta\theta_l^{sc})^2]^{1/2} \quad \text{with}$$

$$\delta q_t^{sc} = \kappa\frac{\overline{w'q_t'}_0}{w_{sc}^*}, \qquad \delta\theta_l^{sc} = \kappa\frac{\overline{w'\theta_l'}_0}{w_{sc}^*}$$

$$\sigma_s^{b} = [(a\delta q_t^{b})^2 + (b\delta\theta_l^{b})^2]^{1/2} \quad \text{with}$$

$$\delta q_t^{b} = \kappa\frac{\overline{w'q_t'}_0}{w^*}, \qquad \delta\theta_l^{b} = \kappa\frac{\overline{w'\theta_l'}_0}{w^*}. \tag{17}$$

Here κ is a proportionality constant, and w_{sc}^* and w^* are convective velocity scales for the subcloud circulation [e.g., $(g/\theta_0\int_0^{z_t}\overline{w'\theta_v'})^{1/3}$ with z_t the top of the subcloud layer] and full layer, respectively. Arguably σ_s^b should include some contribution from the entrainment fluxes at cloud top as well as from the surface fluxes, but we have kept the given form for simplicity.

3. Comparison with LES results

The LES results we will compare to were all generated with the same LES model employed in Lewellen and Lewellen (1998, hereafter referred to as LL98), described there and in references therein. The simulations considered fall into two categories: an idealized set generated for the study in LL02, and a more ''realistic'' set representing our contributions to recent LES intercomparisons organized by the GCSS-WG1. For convenience, the conditions for the cases that are featured most prominently in the later figures are briefly summarized in the table in appendix B.

The first set includes results from more than 30 simulations described in LL02 of idealized boundary layers driven solely by prescribed heat and moisture fluxes (see appendix B in LL02 for a full summary). All the layers were ''tightly capped,'' that is the inversion layer thickness was much smaller than the boundary layer depth. This was achieved in some cases using true inversions with large temperature jumps, and in others through the artifice of a rigid lid placed at the top of the layer with a negative heat flux (and a zero or positive moisture flux) forced through it to build up a thin inversion layer immediately below the lid. The principal variations considered were in the magnitude of the surface fluxes, the cloud-top humidity and temperature jumps, and the relative cloud depth. The set was designed in particular to sample the transition from nearly horizontally uniform clouds to shallow cumulus.

The second set includes the four most recent GCSS-WG1 intercomparison cases, all based on particular sets of field observations: a low cloud fraction shallow cumulus case (Siebesma et al. 2003) based on data from the Barbados Oceanographic and Meteorological Experiment (BOMEX); a higher cloud fraction cumulus case (Stevens et al. 2001) based on data from the Atlantic Trade Wind Experiment (ATEX); a diurnal cycle of shallow cumulus over land (Brown et al. 2002) based on data taken at the Atmospheric Radiation Measurement (ARM) site; and, as part of the European Project on Cloud Systems in Climate Models (EUROCS), a diurnal cycle of marine stratocumulus (Duynkerke et al. 2003, manuscript submitted to *Quart. J. Roy. Meteor. Soc.*) based on observations taken during the First International Satellite Cloud Climatology Project (ISCCP) Regional Experiment (FIRE) off the California coast. In each case the LES intercomparisons showed good agreement between different LES models, providing a robust target for the testing of simpler models or relationships; the results from our LES were entirely representative.

Figures 1–4 show sample comparisons between model predictions and LES results. Each case considered is represented by a pair of figure panels. The left member shows the LES mean cloud fraction (thin solid line) and $\hat{R}$ profile from (10) (thick solid line) compared with the predicted $\hat{R}$ profile from (11) (thin short dash) and with the correction in (16) (thick long dash). The right member shows the corresponding LES and predicted buoyancy fluxes using the same dash patterns. The LES results are of 1- or 2-h averages about selected times. The $\hat{R}$ comparison is based on the form in (10) rather than in (7) because the exact saturation deficit flux was not collected during the simulations, but $\overline{w'\theta_v'}$, $\overline{w'\theta_l'}$, and $\overline{w'q_t'}$ were.

The agreement between predictions and LES results is, in general, excellent. The results from the rest of the LES dataset of LL02 (in all three regimes identified

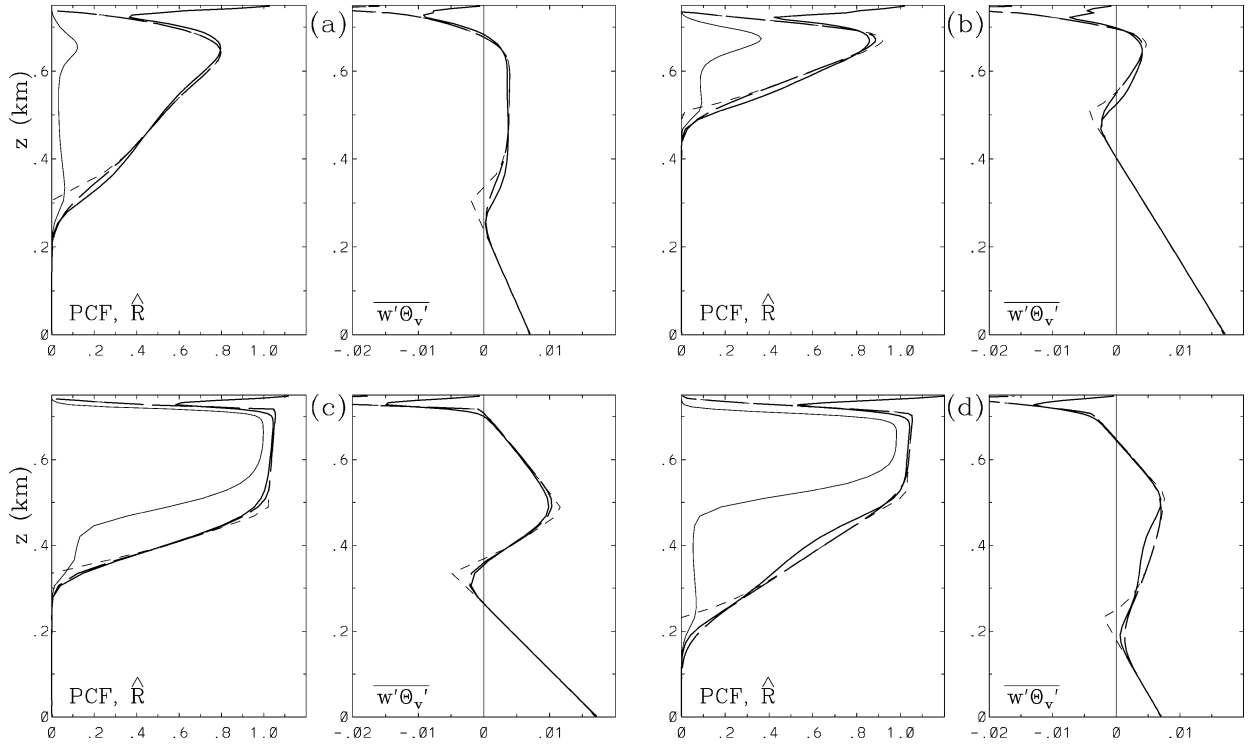

FIG. 1. Mean vertical profiles from sample cloudy boundary layers considered in LL02, cases (a) R1, (b) R4, (c) R8, and (d) M1. Solid lines in the left panel of each pair are the LES results for partial cloud fraction (thin line) and $\hat{R}$ (thick line), and in the right panels virtual potential temperature flux (in K m s^{-1}). Thin short dashed lines are predicted profiles using Eq. (11); thick long dashed lines are the predictions including the correction in Eq. (16).

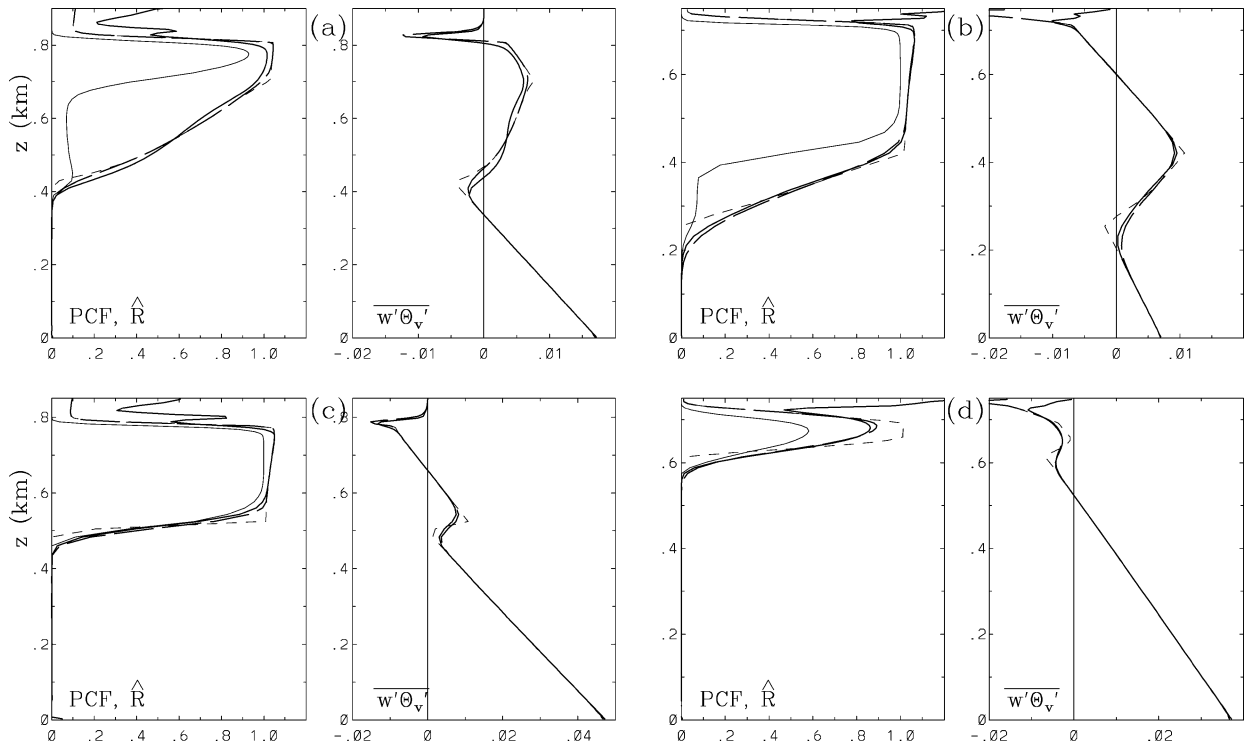

FIG. 2. Mean vertical profiles from sample cloudy boundary layers considered in LL02, cases (a) NHb, (b) T0, (c) N2, and (d) T5. Lines and variables as in Fig. 1. Note changes in scales between plots.

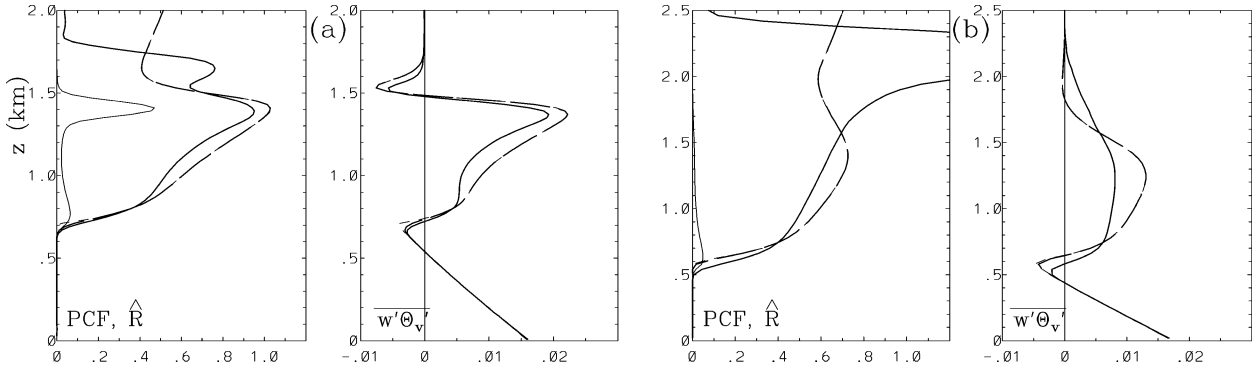

FIG. 3. Mean vertical profiles from (a) ATEX and (b) BOMEX GCSS-WG1 cases. Lines and variables as in Fig. 1.

there) are in comparably good agreement, as are the GCSS cases at different times than those shown. The conditions represented are quite varied, including: a convective boundary layer with a growing partial cloud layer (Fig. 2d); stratocumulus boundary layers driven by surface fluxes (Fig. 2c), driven by cloud-top radiative cooling (Fig. 4b), and exhibiting solar-induced afternoon decoupling (Fig. 4a); quasi-steady shallow cumulus underlying stratocumulus with different cloud depths, cloud fractions, surface fluxes, and cloud-top conditions (Figs. 1a–d and 2a,b); somewhat deeper cumulus for both quasi-steady (Figs. 3a,b) and strongly time-varying (growing and collapsing) conditions (Figs. 4c,d).

For the results shown in these and subsequent figures we have set q_t^{sc} and θ_l^{sc} equal to the average of the mean measured profiles over the bottom quarter of the subcloud layer; $\kappa = 2$ has been used in (17) for estimating the fluctuation contribution. The results prove to be fairly insensitive to the precise choice of subcloud parcel properties; the chief differences appear near cloud base due to the change in lifting condensation level. The

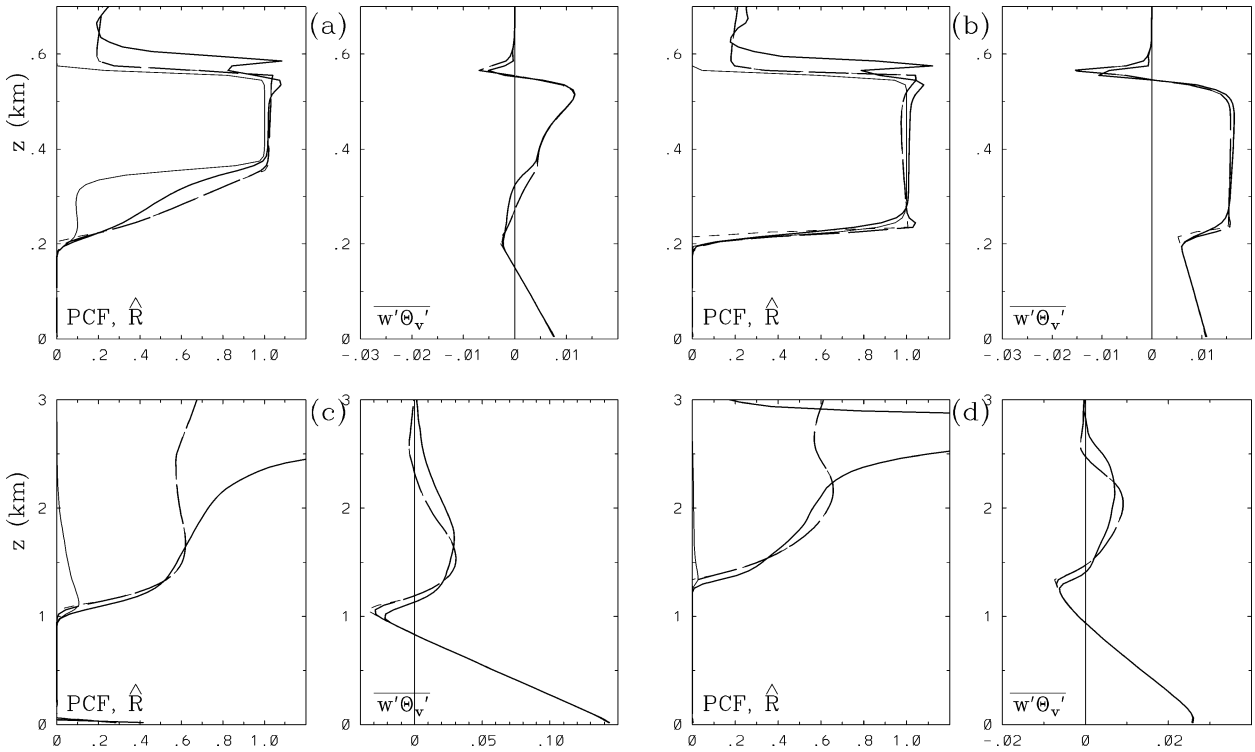

FIG. 4. Mean vertical profiles from GCSS-WG1 cases: (a) EUROCS diurnal simulation of stratocumulus at simulation hour 14 [1400 local time (LT)] and (b) at hour 26 (0200 LT); (c) ARM case at simulation hour 8 (1330 LT) and (d) at hour 12 (1730 LT). Lines and variables as in Fig. 1. Note changes in scales between plots.

improvement from the inclusion of fluctuations via (16) is modest (sometimes negligible; e.g., figs. 3a,b and 4c,d) but consistent, with the biggest effect around cloud base for shallower boundary layers. Again the results are relatively insensitive to the precise choice of fluctuation levels, justifying the rough treatment afforded in (17). In several cases the $\hat{R}$ and $\overline{w'\theta'_v}$ predictions with the (16) term included are nearly indistinguishable from the LES profiles.

We note in passing several other features apparent in the figures. 1) As advertised, $\hat{R}$, which from (6) may be interpreted as an effective cloud fraction, can be much greater than the actual mean cloud fraction when cumulus columns are present. 2) Generally for cumulus-coupled layers $\hat{R}$ rises approximately linearly with height in the region with column clouds, reaching the value 1 if and when the mean cloud fraction exceeds one-half. 3) In cases with thick solid cloud layers the predicted and measured $\hat{R}$ often modestly exceed 1; this a consequence of the approximation made in going from (3) to (4) and, correspondingly, using (11) instead of (9). The excess above 1 observed in the figures in these cases represents the largest differences encountered between the alternative formulations (9) and (11). 4) Above z_i the fluxes approach 0, therefore the measured $\hat{R}$, determined by a ratio of fluxes, becomes inaccurate and eventually undefined. 5) In the BOMEX and ARM GCSS examples the LES-measured $\hat{R}$ is observed to significantly exceed 1 in the upper part of the layer. These are the only cases presented with very weakly capped cumulus layers, and the large values trace to regions with overshooting cumulus tops where there can be both clear and cloudy updrafts at the given height. The simple picture of section 2, which assumes all updrafts to be clear or all to be cloudy at a given height, does not attempt to include these effects. 6) The wet and dry buoyancy fluxes, W and D, are often of opposite sign and comparable magnitude, so from (6) a small relative change in $\hat{R}$ often leads to a larger relative change in $\overline{w'\theta'_v}$. 7) The effects of neglecting lateral mixing into the updraft plumes may just be apparent for some of the deeper cumulus layers (particularly the BOMEX case). In the interesting regime where $0 < \hat{R} < 1$, (9) reduces to $\hat{R} = q_l^{sc}/(q_l^{sc} - s^b)$; the leading effect of lateral mixing is to reduce the updraft liquid water q_l^{sc} by some amount δq_l, a change which will appear in both numerator and denominator. For this to make a significant difference in the ratio we must have that δq_l is significant compared with q_l^{sc} *and* that s_b is significant compared with $q_l^{sc} - \delta q_l$. In other words we expect that not including mixing corrections may lead to an overestimate of $\hat{R}$ for cases with tall cumulus columns and large saturation deficits in the background flow. 8) In Fig. 4b near cloud base the measured $\hat{R}$ is less than the measured cloud fraction, while the predicted $\hat{R}$ is greater (as in other cases). While the discrepancy is minor, this suggests that for layers such as this one driven dominantly by downdrafts (e.g., radiatively cloud-top cooled stratocumulus with little or no surface forcing) one should consider using downdraft parcels in the formulation rather than (or in addition to) the updraft parcels originating in the subcloud layer that were used.

4. Applications to entrainment and flux predictions for shallow cumulus

The results of the last section demonstrate a strong correlation between the mean θ_l and q_t profiles and $\hat{R}$. It is tempting to employ this in the coupling of a fully predictive single-column model (e.g., a higher-order closure model), using the current $\overline{\theta_l}$ and $\overline{q_t}$ at each time step to determine $\hat{R}$ and thence the buoyancy flux. However, a good correlation between variables is insufficient to guarantee that a coupling will be well behaved in a model: cause and effect must be properly represented in the implementation or else small errors will grow and the model predictions wander away from physical reality. If the physics determining the θ_l and q_t profile shapes is not properly represented in the model then the suggested determination of $\hat{R}$ will ultimately perform poorly.

It was argued in LL02 that the feedback between large-scale circulation structure and entrainment into the boundary layer from above is a critical ingredient in determining the quasi-steady properties a layer will equilibrate to, including the θ_l and q_t profile shapes. The remainder of this paper explores this issue further for cumulus-coupled layers: first, using $\hat{R}$ to extend the entrainment parameterizations presented in LL98 and LL02 to partly cloudy layers; and second providing an indirect test of the postulated feedback by showing that it can lead to good a priori predictions for quasi-steady cumulus-coupled layer dynamics.

a. Entrainment efficiency for partly cloudy conditions

In LL98 we considered a large-eddy entrainment efficiency [closely related to the entrainment parameterization of Stage and Businger (1981)],

$$\eta = \int (\overline{w'\theta'_{v\mathrm{NE}}} - \overline{w'\theta'_v})\, dz \Big/ \int \overline{w'\theta'_{v\mathrm{NE}}}\, dz, \quad (18)$$

where $\overline{w'\theta'_v}$ is the actual buoyancy flux profile in the layer and $\overline{w'\theta'_{v\mathrm{NE}}}$ is that buoyancy flux that would result if the entrainment process being considered were not present. The numerator represents an estimate of the energetic cost of entrainment incurred by the buoyantly driven layer-scale circulation; the denominator is an estimate of the energy input available to drive the circulation. The working assumption, supported by LES results (LL98; Lewellen and Lewellen 2000; LL02), is that for buoyantly driven quasi-steady layers the cloud-top entrainment rate is set by the upper limit that the large-scale circulation can energetically support.

Computing η for a given case, or using (18) to predict entrainment by assuming a given value for η, both require knowledge of $\overline{w'\theta'_{v\mathrm{NE}}}$. As discussed in LL98, for quasi-steady conditions the ''no entrainment'' fluxes of the conserved variables θ_l and q_t can be estimated given the surface fluxes and the contributions (if any) from large-scale advection, radiation, or precipitation. If the latter effects are absent, the quasi-steady $\overline{w'\theta'_{l\mathrm{NE}}}$ and $\overline{w'q'_{t\mathrm{NE}}}$ profiles are simply linear from their surface values to 0 at the inversion height, z_i. LL98 concentrated on layers with approximately horizontally uniform cloud layers so that $\overline{w'\theta'_{v\mathrm{NE}}}$ follows from $\overline{w'\theta'_{l\mathrm{NE}}}$ and $\overline{w'q'_{t\mathrm{NE}}}$ using (2) or (4). Employing $\hat{R}$ these results can be extended to partly cloudy boundary layers, in particular cumulus-coupled layers, using (6) to relate the no-entrainment fluxes.

LL02 employed the large-eddy entrainment efficiency and a simple classification of circulation structures to study the ''decoupling'' transition leading to a cumulus-coupled boundary layer. Starting from three basic eddy scales (full layer, cloud layer, subcloud layer) we defined three idealized circulation regimes (I, II, III) depending on which eddy type was hypothesized to limit the entrainment flux transport. In regime I the flux transport is driven by full-layer-scale eddies (e.g., as in the dry convective boundary layer). In regimes II and III the entrained flux is transported across the full layer in two steps, first by cloud-scale, then by subcloud-scale eddies. In quasi-steady state (i.e., with the shapes of the θ_l and q_t profiles approximately constant in time) the flux transport in the upper and lower circulations equilibrates by weakening the stronger circulation or strengthening the weaker. In regime II (identified with a class of stratocumulus layers) the cloud deck is assumed solid and the entrained flux is the maximum that the upper circulation can support; the subcloud layer is only partially capped with stronger plumes passing through, but with the downward circulation still sufficient to mix the entrained fluxes across that layer. In regime III (identified with cumulus coupling), the subcloud layer transports the maximum entrainment flux it can support (it is effectively capped, behaving as a dry convective layer), while the upper circulation is weakened by a drop in cloud fraction over at least part of the depth of the layer (leading to the appearance of column clouds).

Beginning in regime III and increasing the surface sensible heat flux, for example, augments the lower circulation relative to the upper and a transitional period follows in which the subcloud layer heats and dries faster than the upper layer, reducing the column cloud depth until equilibrium is restored. A big enough change eliminates the column cloud and drives the system into II where the upper circulation has trouble keeping up with the lower; the lower circulation overentrains relative to the upper, weakening the capping of the lower layer until equilibrium is restored with the stronger subcloud plumes exiting the layer. With a large enough increase in the surface sensible heat flux the circulation will become organized more into a full-layer circulation and the regime I picture becomes more appropriate.

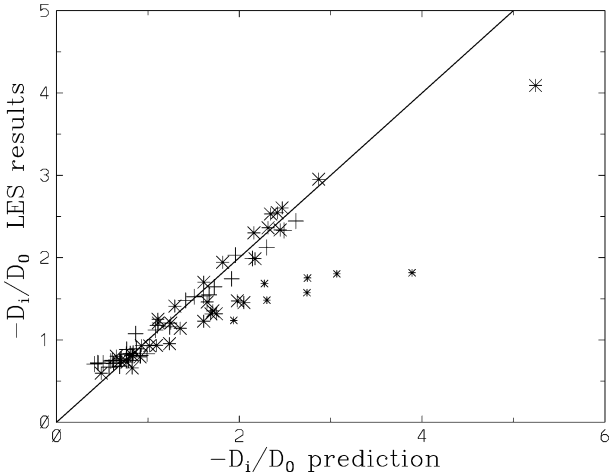

FIG. 5. Normalized LES-measured entrainment flux vs that predicted based on the cloud-layer circulation dynamics. Points from the regime II (pluses) and regime III (large and small stars) datasets from LL02. Small stars are from case R8 discussed in the text.

In LL02 the cloud-top entrainment in the quasi-steady cumulus regime (III) was predicted by applying (18) to the subcloud circulation, and found in good agreement with LES results. We now apply (18) to the upper circulation, to check whether using $\hat{R}$ to determine $\overline{w'\theta'_{v\mathrm{NE}}}$ for a partly cloudy circulation gives an entrainment efficiency consistent with our previous results. An advantage of the entrainment prediction based on the cloud circulation is that it could be used even if the upper and lower circulations had not yet equilibrated, in which case the prediction based on the subcloud circulation would not be correct. The predicted versus LES-measured results for the entrainment dry buoyancy flux, D_i, normalized by the surface flux, D_0, are shown in Fig. 5 for the entire regime II and III datasets from LL02. The details of the application of (18), assumed entrainment efficiency ($\eta = 0.55$), and plot format are all as in LL02; the $\hat{R}$ used is that measured from the LES results. The agreement is generally quite good.

The data points with the poorest agreement are from a single LES run, R8, at different times. In this case a vertically uniform large-scale advective cooling term was included so that the cloud thickness grew in time even though the mean cloud-top conditions were close to the nominal buoyancy-reversal threshold. Within the bulk of the cloud layer there is little difference between $\overline{w'\theta'_v}$ and $\overline{w'\theta'_{v\mathrm{NE}}}$ as currently computed, so that the perceived entrainment cost is largely contributed from the regions around cloud base and cloud top. There are probably local regions of buoyancy reversal in this simulation (where entrainment would drive, rather than inhibit, the cloud-layer circulation) that should probably

be included in the estimate of the total energy input available to drive the circulation, $\int \overline{w'\theta'_v}_{\mathrm{NE}}$. This would tend to improve the predictions in this case, though we do not know how to include this contribution quantitatively; this effect would be less important or absent over the rest of the dataset where the upper cloud layer is thin or broken, or the cloud-top conditions are not close to the buoyancy-reversal threshold.

b. *Predicting the quasi-steady-state behavior of a shallow cumulus-coupled layer*

Consider the problem of predicting the quasi-steady-state behavior of a cloudy boundary layer given only a minimal set of input parameters: the surface fluxes ($\overline{w'\theta'_l}_0$ and $\overline{w'q'_t}_0$); the $\overline{\theta_l}$ and $\overline{q_t}$ jumps across the top of the layer at z_i; mean subcloud θ_l and q_t values; and specified vertical profiles of sources of θ_l and q_t within the layer, if present (e.g., radiation or precipitation fluxes or large-scale advective forcing). In LL02, predictions were formulated for the cloud-top entrainment fluxes and basic circulation type as functions of these input parameters. In a quasi-steady boundary layer this suffices to determine the conserved fluxes $\overline{w'\theta'_l}$ and $\overline{w'q'_t}$ to a good approximation. For dry-convective or stratocumulus layers this, in turn, largely suffices to provide a characterization of the complete layer dynamics, since to a reasonable approximation the θ_l and q_t profiles within the layer are well mixed, the cloud layer horizontally uniform, and the buoyancy flux determined by the simple limits (2) or (4). For a cumulus-coupled layer, however, these approximations no longer hold; a critical component of the layer dynamics is not yet determined.

In LL02 it was argued that in the cumulus-coupled regime the θ_l and q_t profiles will naturally dynamically adjust, altering the cloud structure and hence the buoyancy flux, until the entrainment fluxes at cloud top driven by the upper circulation are in equilibrium with what the subcloud circulation can support. Consider, for example, an initially horizontally uniform cloud cover, with θ_l and q_t well mixed, in a boundary layer that the analysis of LL02 predicts will be cumulus coupled if in a quasi-steady state. In this case the upper, cloudy circulation can support a larger entrainment flux across cloud top than the lower, subcloud circulation can transport through the subcloud layer. Consequently, the upper layer warms and dries relative to the subcloud layer and the cloud base becomes nonuniform (a raised general base with narrow column clouds below). The change in cloud structure reduces the buoyancy flux driving the upper circulation and thereby the cloud-top entrainment flux. This development proceeds until the entrainment flux driven by the upper circulation is reduced enough to be in equilibrium with what the subcloud circulation can support.

This picture suggests that for a quasi-steady cumulus-coupled layer the equilibration of the upper- and lower-layer entrainment predictions should be used in predicting the buoyancy flux profile in terms of the chosen input parameters. Further assumptions are required since equating the two entrainment predictions provides only a single constraint, insufficient for determining a vertical profile. We proceed by postulating a one-parameter family of solutions within the cloud layer, then use the entrainment constraint to choose from among this family. The hope is that if the key dynamical feedbacks are as postulated, then the solution will perhaps be forgiving of the errors necessarily associated with this level of approximation.

As in LL02 the entrainment prediction from the subcloud circulation in the cumulus-coupled regime is used to predict the entrainment fluxes and thereby the quasi-steady $\overline{w'\theta'_l}$ and $\overline{w'q'_t}$ profiles. Given $\hat{R}$, these could be used to obtain $\overline{w'\theta'_v}$. Determining $\hat{R}$ as suggested in section 2 requires $\overline{\theta_l}$ and $\overline{q_t}$ profiles. These are assumed known in the subcloud layer (except near its top, z_t, in the ''transition layer'') and above z_i. Empirically, we find that across the bulk of the cloud layer θ_l is often approximately linear in z (though this admittedly ignores meaningful structure one might hope to incorporate). For simplicity, then, we consider a one-parameter family of θ_l profiles which is linear across the bulk of the cloud layer, with quadratic interpolations above and below (in the inversion and transition layers) to match onto the known profile above z_i and well below z_t. The q_t profile is then chosen to be consistent with the θ_l profile and predicted $\overline{w'\theta'_l}$ and $\overline{w'q'_t}$ profiles by using the mass flux prescription (8) at the same rough level of treatment as in section 2. The assumed forms of the θ_l and q_t profiles are given explicitly in appendix C.

The one-parameter family of solutions is sampled in Fig. 6 for case NHb from LL02 (cf. Fig. 2a) along with the member of that family satisfying the upper-circulation entrainment constraint, and the LES profiles. The successful prediction of $\overline{w'\theta'_l}$ and $\overline{w'q'_t}$ follows from the success of the entrainment prediction from the subcloud circulation (detailed in LL02) and the quasi-steady approximation. Given the limitations of the one-parameter family of θ_l profiles chosen, the predictions for the $\overline{\theta_l}$, $\overline{q_t}$, $\hat{R}$, and $\overline{w'\theta'_v}$ profiles capture the basic structure of the quasi-steady LES results quite well.

Repeating this exercise for all of the cumulus-coupled cases in LL02 gives comparable results, with the exception of case R8 discussed above. Figure 7 shows the $\hat{R}$ and $\overline{w'\theta'_v}$ predictions obtained in this way for the subset of LL02 cases that were included in Fig. 1. For case R8 (Fig. 7c) the predictions favor a thinner stratocumulus layer overlying the cumulus columns than is found in the LES results; the simulation time shown (as in Fig. 1c) is that for which the entrainment prediction in Fig. 5 is poorest.

Figure 8 shows the analogous predictions for the ATEX and BOMEX GCSS-WG1 cases. In these simulations there were additional contributions from large-scale advective forcing, radiation, and subsidence.

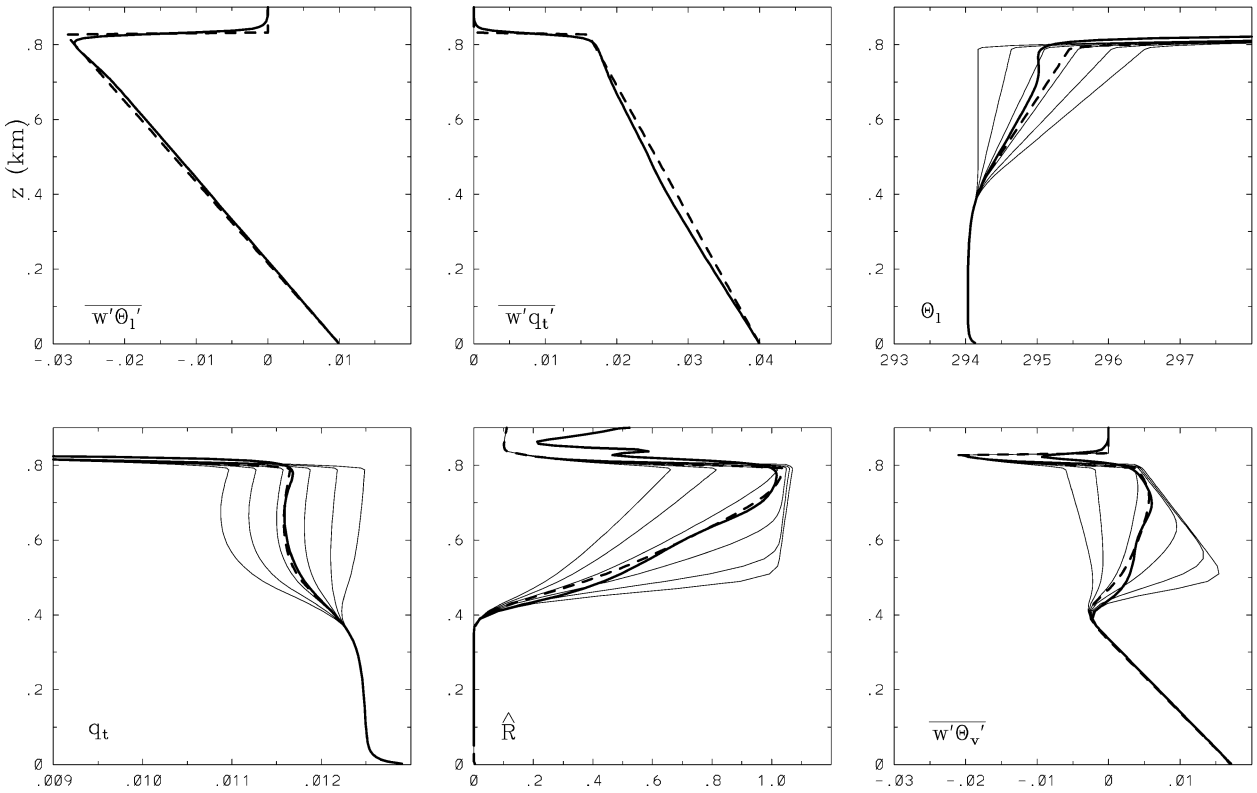

FIG. 6. Sample mean vertical profiles for case NHb from LL02. Thick solid lines are LES results; thin solid lines are sample members of the one-parameter family of approximate solutions discussed in the text; thick short dashed lines are the predicted members of this family satisfying the entrainment constraints, as discussed in the text.

These effects were included in predicting $\overline{w'\theta_l'}$ and $\overline{w'q_t'}$ in this exercise, using the forcings prescribed for the LES intercomparison and, for the ATEX case, the quasi-steady radiative cooling profile found in our LES results. The predictions are again reasonable for these deeper layers, though not as good as for the LL02 dataset. The predictions were made using the approximation of a sharply capped layer; for the BOMEX case in particular this is not a very good approximation.

Analogous predictions based on a piecewise linear one-parameter family of $\hat{R}$ profiles generally matched the LES results even better (particularly for the ATEX and BOMEX cases), but without providing any prediction for the θ_l and q_t profiles.

5. Concluding remarks

In this work an approximate formulation for the horizontal mean buoyancy flux within a partly cloudy boundary layer has been developed in terms of the liquid potential temperature and total water fluxes, requiring only the mean θ_l and q_t profiles as additional information. Comparison with a broad range of LES results has shown that the formulation does a good job representing the buoyancy flux, bridging between the limits of layers that are well characterized by joint-Gaussian pdfs and cumulus-coupled layers with strongly correlated clouds and updrafts and very low cloud fractions. The formulation has the advantage of not requiring knowledge of less accessible quantities such as the mean liquid water, cloud fraction, saturation variance, or vertical velocity skewness, as in related formulations (e.g., Bechtold and Siebesma 1998; Cuijpers and Bechtold 1995; Lewellen and Yoh 1993).

The formulation performs particularly well for transitional layers in between uniform stratocumulus and well-developed shallow cumulus. The behavior in such cases (e.g., cumulus under stratocumulus) differs from that predicted by the formulation of Bechtold and Siebesma (1998), which has been empirically fit to the limits of very high or very low cloud fraction. In the present formulation there is not a one-to-one correspondence between the effective cloud fraction $\hat{R}$ and the mean cloud fraction; the underlying dynamical regime is important and is reflected in the structure of the θ_l and q_t profiles. This conclusion is supported by the LES results. For example, Fig. 9 shows a scatterplot of LES results for $\hat{R}$ versus mean partial cloud fraction (pcf). The points are taken at each vertical grid level from mean profiles from the full LL02 simulation set

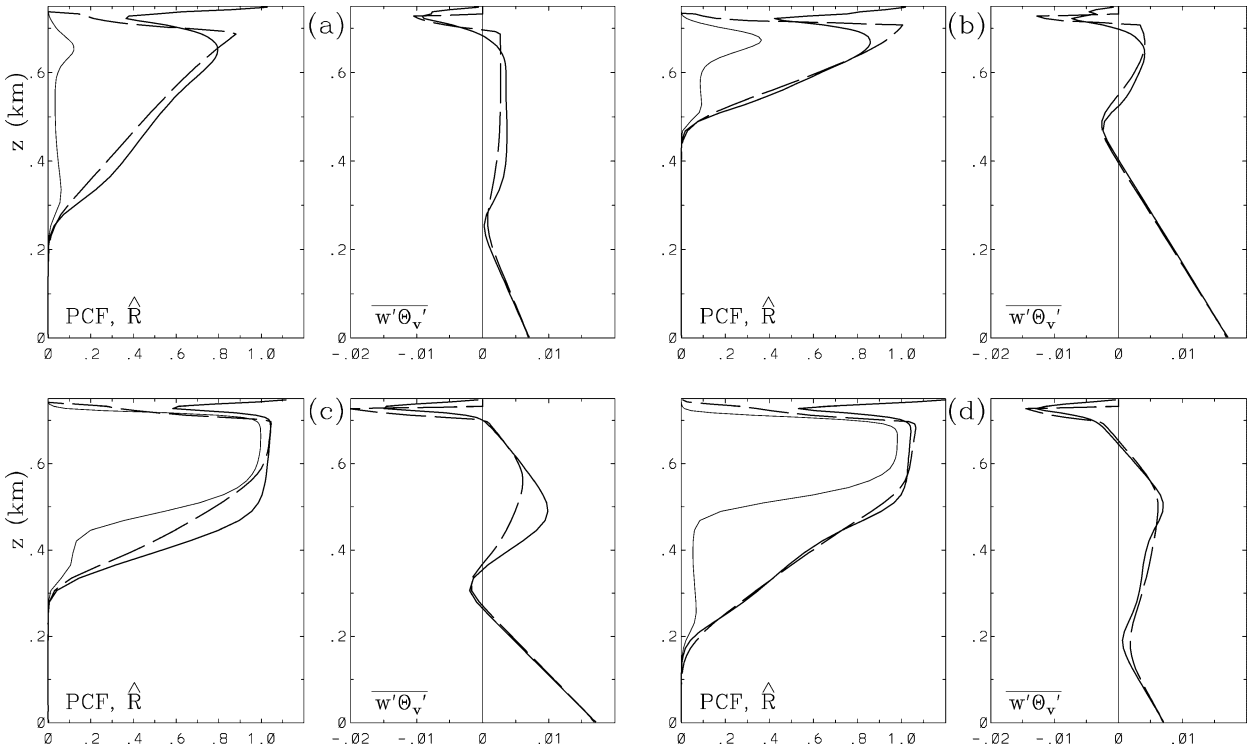

FIG. 7. As in Fig. 1 but with the predictions (long dashes) made using the entrainment constraints as discussed in the text.

plus the ATEX, BOMEX, EUROCS, and ARM cases (including a full sequence of 1-h averages through the diurnal cycles of the latter two cases). The solid line is the prediction from Bechtold and Siebesma (1998; adapted from their Figs. 4 and 6). The scatterplot does not support a one-to-one correspondence between $\hat{R}$ and pcf. Both the cumulus (low pcf) and Gaussian ($\hat{R}$ = pcf) branches considered by Bechtold and Siebesma (1998) are well populated, but so are other regions. In the binormal model of Lewellen and Yoh (1993) $\hat{R}$ and pcf are not predicted to be in one-to-one correspondence; each is a function of $\overline{s}/\sigma_s$ [as in Bechtold and Siebesma (1998)] but also functions of skewness. The predicted $\hat{R}$ versus pcf curve shifts up and to the left with increasing skewness. For example, the dashed line in Fig. 9 is the binormal model prediction using skewness (of both s and w) = 3, while the skewness = 0 prediction is the $\hat{R}$ = pcf line. In the LES results, we find that there is a general trend toward increasing $\hat{R}$ with increasing w-skewness (at fixed pcf), particularly within an individual simulation, but even for fixed w-skewness $\hat{R}$ and pcf are not found to be in one-to-one

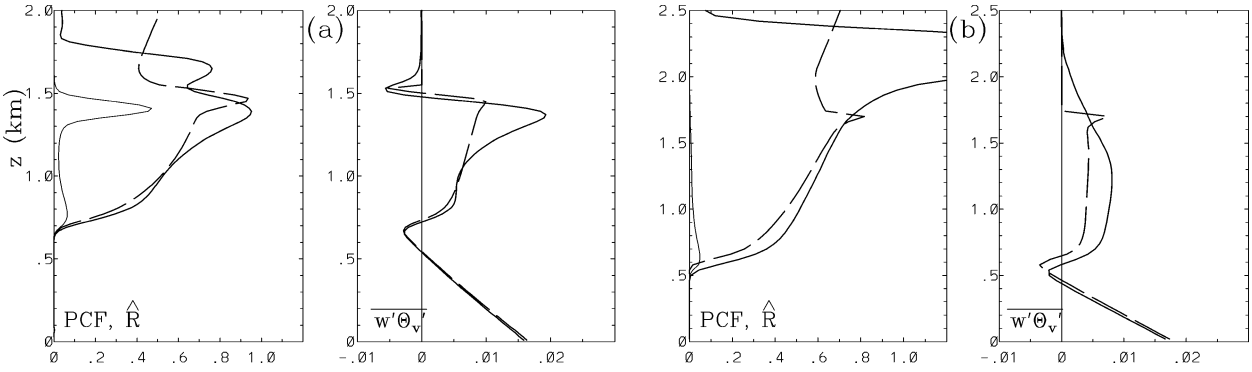

FIG. 8. As in Fig. 3 but with the predictions (long dashes) made using the entrainment constraints as discussed in the text.

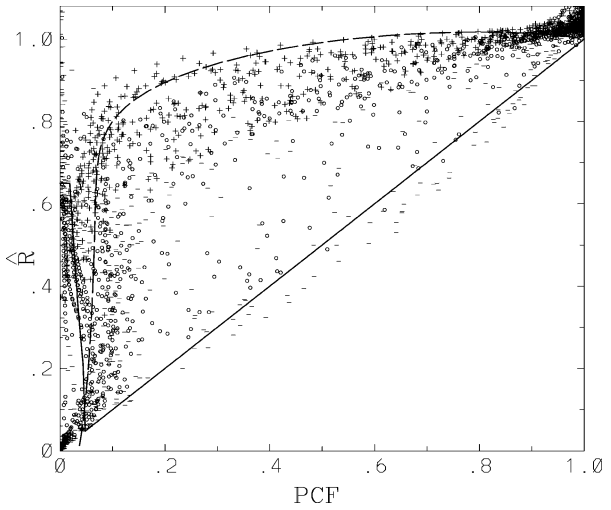

FIG. 9. Scatterplot of LES results for $\hat{R}$ vs partial cloud fraction with the different symbols indicating the vertical velocity skewness interval (''−'' if less than 1, ''o'' between 1 and 3, ''+'' if greater then 3). The solid line is the prediction from Bechtold and Siebesma (1998), the dashed line the prediction of Lewellen and Yoh (1993) for skewness = 3.

correspondence. Besides $\overline{s}/\sigma_s$ and w-skewness other parameters, such as differing values of s-skewness, must come into play; in a given region of the $\hat{R}$ versus pcf plot, the w-skewness can vary significantly. These results (following from a more detailed analysis of the LES results) can be seen in a rough way in Fig. 9, where we have used different symbols to indicate whether the w-skewness at that point is less than 1, between 1 and 3, or greater than 3.

Even though the comparison between LES results and the $\hat{R}$ formulation of section 2 is generally very good, there are possibilities for improvements or additions to the basic formulation that may be worth exploring. In particular, motivated by a simple mass flux picture, the leading effects of the lateral mixing into updrafts could be included and/or a small number of different parcels could be sampled. This could lead to improved treatment of cumulus layers with weaker, more vertically smeared capping inversions.

This formulation for the buoyancy flux was used to extend our previous work on entrainment and quasi-steady structure in cloudy boundary layers (LL02): first using it to apply a large-eddy entrainment efficiency to predict entrainment rates for partly cloudy cumulus layers; and second, using this result to predict the equilibrium structure (particularly the $\overline{\theta_l}$, $\overline{q_t}$, and flux profiles) for those layers. Again the predictions agree well with the LES results.

The success of these predictions for many different cases supports the underlying picture advocated in LL02 of the physical balances responsible for the quasi-steady behavior in shallow cumulus layers. We emphasize in particular how much is being predicted from a minimal set of physical inputs, without invoking a posteriori features of the LES results such as the buoyancy flux, cloud fraction, entrainment rate, or temperature and moisture differences between the cloud and subcloud layers. This evidence for a large-scale balance constraining the buoyancy flux may in part explain the results from LES studies (e.g., Brown 1999) showing an insensitivity to resolution and subgrid model of the mean flux profiles for quasi-steady cumulus simulations even though the structure of the individual cumulus plumes shows a clear sensitivity. Our primary focus on quasi-steady boundary layers here is based on the belief that an understanding of the physical balances involved in quasi-steady layers is a critical ingredient required to construct simple models that can more robustly treat the evolution between different boundary layer regimes.

Finally, we would caution in implementing the suggested formulation for the buoyancy flux within a boundary layer model that the appropriate physics must be included in that model to ensure a good representation of $\overline{\theta_l}$ and $\overline{q_t}$ in different dynamical regimes or else the overall results may not be satisfactory. In particular, as has been emphasized in the literature (e.g., Bretherton and Wyant 1997; LL02) and as our quasi-steady predictions here demonstrate, cloud-top entrainment heating and drying plays a critical role in setting up the ''decoupled'' θ_l and q_t profiles characteristic of cumulus-coupled dynamics.

Acknowledgments. This work was supported by Grant N00014-98-1-0595 from the Office of Naval Research with R. Ferek as technical monitor. We would also like to thank the GCSS Working Group 1 for its influence in stimulating this work, and for the comments of three anonymous reviewers that led to improvements in the presentation.

APPENDIX A

Thermodynamic Coefficients

The thermodynamic coefficients used in the text are as in Cuijpers and Bechtold (1995); they are listed here for convenience.

$$a = (1 + L\overline{q}_{\mathrm{sl},T}/c_p)^{-1}, \qquad b = a(\overline{T}/\overline{\theta})\overline{q}_{\mathrm{sl},T},$$

$$c = a(\overline{q_t} - \overline{q}_{\mathrm{sl}}), \qquad \alpha = 0.61\overline{\theta},$$

$$\beta = (\overline{\theta}/\overline{T})(L/c_p) - 1.61\overline{\theta},$$

with the saturation specific humidity defined as $\overline{q}_{\mathrm{sl}} = q_s(\overline{T}_l)$ for $\overline{T}_l = \overline{\theta}_l(\overline{T}/\overline{\theta})$, and $\overline{q}_{\mathrm{sl},T} = \partial q_s/\partial T|_{T=\overline{T}_l} = Lq_s(\overline{T}_l)/(R_v\overline{T}_l^2)$. Here, L is the latent heat of vaporization, c_p the specific heat of air at constant pressure, and R_v the gas constant of water vapor.

APPENDIX B

Table of Simulations

Run	$\overline{w'\theta'_{l0}}$	$\overline{w'q'_{t0}}$	ζ	Rad.	z_i	pcf	Δx	Δz	Domain	Time	Notes
R1	0	4	1.7	none	0.73	0.12	40	5	3.2	2–4	qs, 1
M1	0	4	0.58	none	0.73	0.98	40	5	3.2	2–4	qs, 1
NHb	1	4	1.4	none	0.83	0.52	20	5	3.2	2–4	qs
R4	1	4	1.6	none	0.73	0.34	40	5	3.2	4–6	qs, 1
R8	1	4	1.1	none	0.73	1.0	40	5	3.2	14–16	gc, 1
T0	0	4	0.0	none	0.73	1.0	40	5	3.2	6–8	qs, 1
T5	3	4	0.1	none	0.73	0.58	40	5	3.2	6–8	gc, 1
N2	4	4	0.17	none	0.8	1.0	40	5	3.2	4–6	dc
ATEX	0.7	4.8	1.5	LW	1.5	0.47	100	20	6.4	3–8	qs
BOMEX	0.8	5.2	2.0	fixed	1.7	0.05	100	40	6.4	4–6	qs
EUROCS	0.6, 0.9	0.8, 1.1	0.7	LW+SW	0.57	1.0	50	10	2.5	13–14, 25–26	d
ARM	11, 1	17, 8	3.0	none	2, 2.4	0.08, 0.03	66.7	40	6.4	7–8, 11–12	d

Simulations are represented in Figs. 1–4 and 6–8. Listed are surface heat flux ($\overline{w'\theta'_{l0}}$ in km s^{-1} × 10^{-2}); surface moisture flux ($\overline{w'q'_{t0}}$ in g m g^{-1} s^{-1} × 10^{-5}); cloud-top jump ratio [$\zeta = (L/c_p)\,\Delta q_t/\Delta\theta_l$]; radiation type [none, fixed prescribed profile, coupled longwave (LW) and coupled shortwave (SW)]; inversion height [z_i (km)]; maximum partial cloud fraction (pcf); horizontal grid spacing [Δx (m)]; finest vertical grid spacing [Δz (m)]; domain size (km); and the time averaging interval used in the figures (hours since the beginning of the simulation); notes (qs = quasi-steady, 1 = with top lid, d = diurnal cycle, gc = growing cloud, dc = decreasing cloud). For time-varying cases the numbers given are representative for the times shown in the figures.

APPENDIX C

One-Parameter θ_l and q_t Profiles for Quasi-Steady Cumulus Predictions

A simplified one-parameter family of θ_l vertical profiles are defined as

$$\theta_l(z;\,\lambda) = \begin{cases} \overline{\theta_l}(z) & z \le z_1 \text{ or } z \ge z_i \\ \overline{\theta_l}(z_1) + A_1(z - z_1) + A_2(z - z_1)^2 & \\ \qquad\qquad z_1 < z \le z_2 & \\ \theta_l(z_2;\,\lambda) + \lambda(z - z_2) & \\ \qquad\qquad z_2 < z \le z_3 & \\ \theta_l(z_3;\,\lambda) + \lambda(z - z_3) + A_3(z - z_3)^2 & \\ \qquad\qquad z_3 < z < z_i, & \end{cases} \tag{C1}$$

with

$$A_1 = \left.\frac{d\overline{\theta_l}}{dz}\right|_{z=z_1}, \qquad A_2 = \frac{1}{2}\frac{(\lambda - A_1)}{(z_2 - z_1)},$$

$$A_3 = \frac{\overline{\theta_l}(z_i) - \theta_l(z_3;\,\lambda) - \lambda(z_i - z_3)}{(z_i - z_3)^2},$$

$$z_1 = 0.85 z_t, \qquad z_2 = z_t + 0.1(z_i - z_t),$$

$$z_3 = z_t + 0.9(z_i - z_t).$$

The profile is constructed to be linear across the middle 80% of the cloud layer, with the slope λ the single undetermined parameter. Above and below this region, the given form quadratically interpolates to the measured values at z_i and z_1, smoothly matching onto the slope λ at z_3 and z_2. The lower height, z_1, was chosen sufficiently below the top of the subcloud layer, z_t, as to be in the ''mixed layer'' where ''universal'' convective boundary layer behavior is found (cf. Fig. 6 in LL02).

The corresponding one-parameter family of q_t profiles found from a crude mass-flux approximation is

$$q_t(z;\,\lambda) = q_t^{sc} - \frac{\overline{w'q'_t}(z)_p}{\overline{w'\theta'_l}(z)_p}[\theta_l^{sc} - \theta_l(z;\,\lambda)], \tag{C2}$$

where $\overline{w'q'_t}(z)_p$ and $\overline{w'\theta'_l}(z)_p$ are the q_t and θ_l fluxes predicted in the quasi-steady approximation using the cloud-top entrainment prediction deduced from the subcloud circulation as described in the main text.

REFERENCES

Bechtold, P., and A. P. Siebesma, 1998: Organization and representation of boundary layer clouds. *J. Atmos. Sci.*, **55,** 888–895.

——, C. Fravalo, and J. P. Pinty, 1992: A model of marine boundary layer cloudiness for mesoscale applications. *J. Atmos. Sci.*, **49,** 1723–1744.

——, J. W. M. Cuijpers, P. Mascart, and P. Trouilhet, 1995: Modeling of trade wind cumuli with a low-order turbulence model: Toward a unified description of Cu and Sc clouds in meteorological models. *J. Atmos. Sci.*, **52,** 455–463.

Bougeault, P., 1981: Modeling the trade-wind cumulus boundary layer. Part I: Testing the ensemble cloud relations against numerical data. *J. Atmos. Sci.*, **38,** 2414–2428.

Bretherton, C. S., and M. C. Wyant, 1997: Moisture transport, lower-tropospheric stability, and decoupling of cloud-topped boundary layers. *J. Atmos. Sci.*, **54,** 148–167.

Brown, A. R., 1999: The sensitivity of large-eddy simulations of shallow cumulus convection to resolution and subgrid model. *Quart. J. Roy. Meteor. Soc.*, **125,** 469–482.

——, and Coauthors, 2002: Large-eddy simulation of the diurnal cycle of shallow cumulus convection over land. *Quart. J. Roy. Meteor. Soc.*, **128,** 1075–1093.

Cuijpers, J. W. M., and P. Bechtold, 1995: A simple parameterization of cloud water related variables for use in boundary layer models. *J. Atmos. Sci.*, **52,** 2486–2490.

Lewellen, D. C., and W. S. Lewellen, 1998: Large-eddy boundary layer entrainment. *J. Atmos. Sci.*, **55,** 2645–2665.

——, and ——, 2000: Boundary layer entrainment for different capping conditions. Preprints, *14th Symp. on Boundary Layers and Turbulence,* Aspen, CO, Amer. Meteor. Soc., 80–83.
——, and ——, 2002: Entrainment and decoupling relations for cloudy boundary layers. *J. Atmos. Sci.,* **59,** 2966–2986.
Lewellen, W. S., and S. Yoh, 1993: Binormal model of ensemble partial cloudiness. *J. Atmos. Sci.,* **50,** 1228–1237.
Lilly, D. K., 2002: Entrainment into mixed layers. Part II: A new closure. *J. Atmos. Sci.,* **59,** 3353–3361.
Mellor, G. L., 1977: The Gaussian cloud model relations. *J. Atmos. Sci.,* **34,** 3161–3169.
Randall, D. A., 1987: Turbulent fluxes of liquid water and buoyancy in partly cloudy layers. *J. Atmos. Sci.,* **44,** 850–858.
Siebesma, A. P., and Coauthors, 2003: A large-eddy simulation intercomparison study of shallow cumulus convection. *J. Atmos. Sci.,* **60,** 1201–1219.
Sommeria, G., and J. W. Deardorff, 1977: Subgrid-scale condensation in models of nonprecipitating clouds. *J. Atmos. Sci.,* **34,** 344–355.
Stage, S., and J. Businger, 1981: A model for entrainment into a cloud-topped marine boundary layer. Part I: Model description and application to a cold-air outbreak episode. *J. Atmos. Sci.,* **38,** 2213–2229.
Stevens, B., and Coauthors, 2001: Simulations of trade wind cumuli under a strong inversion. *J. Atmos. Sci.,* **58,** 1870–1891.